Oxid Met (2017) 87:1–10
DOI 10.1007/s11085-016-9667-3

BRIEF COMMUNICATION

Development of 1100 °C Capable Alumina-Forming Austenitic Alloys

M. P. Brady[1] · G. Muralidharan[1] · Y. Yamamoto[1] · B. A. Pint[1]

Received: 30 September 2016 / Revised: 3 November 2016 / Published online: 18 November 2016

Abstract Recently developed alumina-forming austenitic (AFA) alloys based on ~12–32 weight % (wt%) Ni offer an attractive combination of oxidation resistance and creep resistance at relatively low alloy cost. However, they exhibit a transition to internal oxidation and nitridation of Al above ~750–950 °C depending on composition and exposure environment. In order to identify AFA compositions capable of higher-temperature operation for applications such as ethylene cracking, the oxidation behavior of a series of developmental, as-cast nominal Fe–(25–45)Ni–(10–25)Cr–(4–5)Al–1Si–0.15Hf–0.07Y–0.01B wt% base alloys with and without Nb, Ti, and C additions was evaluated at 1100 °C in air with 10% water vapor. Protective alumina scale formation was observed at levels of 35Ni, 25Cr, and 4Al with additions of Nb and C, indicating promise for 1100°C capable cast AFA alloys.

Keywords Alumina · Water vapor · Fe-base alloy · Ni-base alloy

Chromia-scale forming Fe- and Ni-base alloys are widely used in chemical process, energy conversion, and combustion system applications where high-temperature corrosion resistance is required [1, 2]. However, alumina-scale forming alloys can offer substantially improved high-temperature corrosion resistance in many industrially relevant environments, particularly those containing aggressive species such as water vapor, S, and C [1, 2]. This is due in part to the greater thermodynamic stability and slower growth rate of alumina versus chromia [1, 2].

Commercial Ni-base alloys capable of alumina scale formation are available, but quite costly due to their high levels of Ni [2, 3]. Commercial ferritic alumina scale-forming alloys (e.g., FeCrAl class) are also well established and offer excellent

✉ M. P. Brady
bradymp@ornl.gov

[1] Oak Ridge National Laboratory, Oak Ridge, TN 37831, USA

oxidation resistance [4]. However, they have poor high-temperature creep resistance due to their open body-centered cubic (BCC) structure, which severely limits their use in high-temperature structural applications [5]. Oxide dispersion-strengthened (ODS) FeCrAl alloys with excellent creep resistance have been commercially available [6], but are very costly due to the need for powder processing to controllably introduce the strengthening dispersion. Such cost considerations have led to reinvigorated interest in the development of Fe-base, alumina-forming austenitic (AFA) alloys to achieve both alumina scale formation and creep resistance at relatively low alloy cost [7–24].

Recently developed AFA alloys [7–9] have focused in the Fe–(12–32)Ni–(12–20)Cr–(2.5–5)Al weight percent (wt%) base composition range. Utilizing $M_{23}C_6$ and/or MC strengthening precipitates (M = Nb) and/or intermetallic second phases (Fe_2Nb base Laves, γ-Ni_3Al, etc.), promising combinations of alumina scale formation and creep resistance have been identified, and scale up and commercialization efforts initiated. However, the necessity to co-balance mechanical properties with oxidation resistance resulted in alloys that exhibited a transition to internal oxidation and nitridation of Al above a critical internal oxidation transition temperature (IOTT), typically in the range of ~750–950 °C depending on the AFA composition range and exposure conditions [25–27].

This IOTT limit for AFA alloys is not an issue for many industrial applications of technological interest, e.g., gas turbine recuperators, heat exchangers, power plant tubing, cast turbine components, etc., which frequently operate in the ~600–900 °C temperature range. It becomes an issue for solid oxide fuel cell balance of plant applications, where operation temperatures can range up to 800–1050 °C, although there are considerable efforts to reduce SOFC operation temperatures to 600–800 °C [28]. However, the IOTT limitations of current AFA compositions makes them unsuitable for technologically important applications such as-cast tubes and components in the petrochemical and chemical process industries where operation in the ≥1000–1100 °C range is required (e.g., ethylene cracking) [3, 29–31]. Alumina-forming alloys are of increasing interest in these applications due to the reported tendency of alumina-forming alloys to be less susceptible to coking effects than chromia-forming alloys in these process environments, thus offering the potential for significantly enhanced durability and operational advantages of reduced downtime [2, 3, 29–33]. The benchmark materials in these applications are cast chromia-forming austenitics and cast alumina-forming Ni-base alloys [3, 29–33]. The goal of the present work was to assess the potential to increase the upper-temperature oxidation limit of cast AFA alloys to the 1100 °C range and identify AFA composition ranges potentially suitable for process environments such as ethylene cracking. The driving force for these alloys is achieving alumina formation at lower Ni levels than currently used Ni-base, cast alumina formers in order to decrease alloy cost.

Selected alloy compositions relevant to designing 1100 °C capable AFA's from a literature search are shown in Table 1 and were used to guide the selection of compositions for study in the present work. The commercial alloy Centralloy® HT E based on 18Fe–45Ni–30Cr–4Al forms protective alumina at >1150 °C and was used as a benchmark to select a maximum Ni level of 45 wt% for investigation [32].

Table 1 Selected alloy compositions (wt%) relevant to Fe/Ni-base alumina-forming alloys

McGurty-type alloys 881-1 and 880-4 [36]	Cast: 881-1 ~Fe–34Ni–10Cr–5Al–0.4Si–0.14Mn–0.019C–0.022Zr–0.005Y; ~880-4 Fe–24Ni–10Cr–5A1–0.4Si–0.14Mn–0.027C–0.026Zr–0.094Y	Alumina former at 1100 °C in air (~1000–2500 h, 20-h cycles). Alloy 880-4 poor 800–900 °C oxidation resistance in air with 10% H_2O [27]
Pivin et al. [34]	Cast/Annealed: Fe–45Ni–25Cr–5Al–Y and [1]Fe–20Ni–20Cr–5A1–Y: range of Y, ~0.02–0.06C, ~0.15Si, ~0.15Mn	Alumina formers at 1200-1300°C in O_2 (< 120 h, isothermal and cyclic).
Belen et al. alloy 36XA [35]	From cast tubes: ~Fe–34Ni–25Cr–3.3Al–1.5Si–1.4Mn–0.8Nb–0.43C	Borderline alumina former at 1000 °C in O_2, internal oxidation < 700 h
Centralloy® HT E [32]	Cast: Fe–45Ni–30Cr–4Al–1Mn–0.8Si–0.5Nb–0.45C	Alumina former > 1150 °C
Brady et al. alloy AFA + Al [27]	Wrought: Fe–25Ni–15Cr–4Al–2.5Nb–2Mn–2Mo–0.15Si–0.1C–0.01B–0.014Hf–0.009Y	Alumina former ≤ ~950 °C air and air with 10% H_2O, internal oxidation > 1000 °C

[1] Likely not single-phase austenitic matrix

Pivin et al. [34] also reported alumina formation at 1200–1300 °C for Fe–45Ni–25Cr–5Al–Y, which led to selection of 25 wt% as the maximum Cr level. Belen et al. [35] reported borderline alumina formation at 1000 °C for alloy36XA with Fe–34Ni–25Cr–3.3Al, therefore a minimum Al level of 4 wt% was selected. The McGurty-type FeNiCrAl alloys reported by Ramakrishnan et al. in [36] formed alumina at 1100 °C in air in the base range of Fe–(25–35)Ni–10Cr–5Al, although a recent study of the 25Ni-base alloy from that work (alloy 880-4) [27] observed poor oxidation resistance in air with 10% H_2O at 800–900 °C despite confirming alumina formation in air at 1100 °C. Recent work involving the present authors observed improved alumina formation, increased IOTT in air with 10% H_2O with increasing levels of Al, Ni, Cr, Nb, C, and B, and a degradation of IOTT with Ti and V, although none of these alloys were capable of alumina scale formation above 900–1000 °C [8, 9, 25–27].

The alloy test matrix in the present work (Table 2) investigated the higher-Ni McGurty-type alloy range, alloy 1: Fe–35Ni–10Cr–5Al base (similar to alloy 881-1

Table 2 Analyzed as-cast alloy compositions in weight percent (wt%) as determined by inductively coupled plasma and combustion techniques (metallic impurities ≤ 0.01 wt% not reported)

Alloy	Fe	Ni	Cr	Al	Nb	Ti	Si	C	Hf	Y	B	S
1	48.51	35.31	9.85	4.94			0.98	0.22	0.14	0.03	0.009	0.001
2	54.63	25.49	14.73	3.94			1.02	0.002	0.14	0.02	0.007	0.002
3	34.73	35.60	24.67	3.93			0.90	0.002	0.12	0.03	0.002	0.001
4	32.99	35.45	24.89	4.11	1.01		1.03	0.3	0.15	0.03	0.006	0.001
5	24.72	45.81	24.44	3.88			0.95	0.004	0.15	0.03	0.006	0.001
6	33.63	35.70	24.51	3.97		0.87	0.85	0.30	0.12	0.03	0.008	0.001

from reference 36). Alloy 2 at Fe–25Ni–15Cr–4Al base was selected as a control for the present authors' current AFA composition range, which exhibits IOTT in the ~850–950 °C range [8, 9, 27]. Alloys 3, 4 [33, 37], and 6 are based on Fe–35Ni–25Cr–4Al to investigate effects of increased Ni and Cr, as well as C, Nb, and Ti additions on IOTT (additions of C and Nb or Ti are needed in this composition range to provide for high-temperature creep strength via carbide phases [35, 37, 39]). The Ni level of Alloy 5 was further increased to 45 wt%, at 25 wt% Cr. All alloys also contained Hf and Y additions in an attempt to optimize alumina formation and adherence [27, 38], and nominal added 0.01B based on current 25Ni-based AFA alloys [26], which appears to enhance alumina formation when water vapor is present.

Table 3 shows the Hf/C and Y/S ratios in atomic % (at.%) for the 6 alloys studied in the present work. In general to optimize alumina scale formation (slow growth rate, increased scale adherence), Hf/C and Y/S should be >1 [38]. All of the alloys exhibited Y/S >1; however, several of the alloys exhibited Hf/C well less than 1 (alloys 1, 4, and 6) due to high levels of C additions (the high C level was an intentional addition in alloys 4 and 6, but an unintended higher than planned impurity in alloy 1). Although high C additions result in suboptimal Hf/C ratios, they are needed to form carbide precipitates to achieve the good creep resistance needed for high-temperature structural use [e.g., 35, 37, 39].

Alloys 1–6 were prepared by arc melting with a non-consumable tungsten electrode using commercially pure elemental feedstock (except for Cr which was high purity to minimize S content), followed by casting in a chilled Cu mold. The castings were nominally 12.5 mm × 12.5 mm cross-section and 75–100 mm in length. Oxidation test samples were electro-discharge machined (EDM) to 20 mm × 10 mm × 1 mm rectangular coupons and prepared to 600 grit (USA standard) finish using SiC grinding paper. Oxidation behavior was studied using 100-h cycles at 1100 °C in filtered compressed dry air with 10 volume percent H_2O added (samples furnace cooled and weighed after every 100-h cycle). Mass change was measured on a Mettler Toledo model XP205 balance (±0.04 mg accuracy). Selected oxidized samples were cut in half using a low-speed diamond saw and cross-sectioned by standard metallographic techniques. Characterization of the oxidized sections was performed by scanning electron microscopy (SEM) with energy-dispersive x-ray analysis (EDS).

Specific mass change data for alloys 1–6 after 1000–1200 h at 1100 °C in air with 10% H_2O are shown in Fig. 1. Net mass loss due to oxide scale spallation was

Table 3 Hf/C and Y/S ratios in at.%, estimated from Table 2 composition analysis

Alloy	at.% Hf	at.% C	Hf/C	at.% Y	at.% S	Y/S
1	0.041	0.97	0.04	0.018	0.002	9
2	0.042	0.009	4.67	0.012	0.003	4
3	0.036	0.009	4.00	0.018	0.002	9
4	0.044	1.315	0.03	0.018	0.002	9
5	0.045	0.018	2.50	0.018	0.002	9
6	0.035	1.312	0.03	0.018	0.002	9

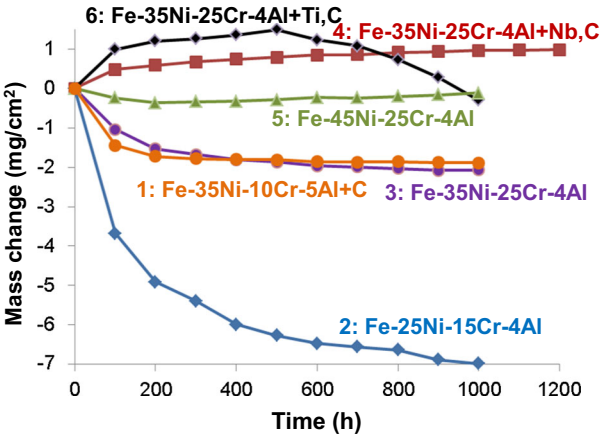

Fig. 1 Mass change at 1100 °C in air with 10% H_2O versus time (100 h cycles) for as-cast Fe–(35,45)Ni–(10,15,25)Cr–(4,5)Al-based alloys with and without C, Nb, and Ti additions

observed for all alloys except for alloy 4: 35Ni–25Cr–4Al + Nb,C which showed low, positive mass gains consistent with protective alumina scale formation. The greatest mass loss was observed for alloy 2: 25Ni–15Cr–4Al, consistent with previous reports of poor oxidation resistance above 850–950 °C in this base composition range [27, 33, 39]. Alloy 1: Fe–35Ni–10Cr–5Al, which was reported to form protective alumina in air exposures at 1100 °C [36], showed mass loss/scale spallation at 1100 °C in air with 10% H_2O, consistent with the degraded oxidation resistance reported for some alumina formers (and chromia formers) in the presence of water vapor or steam [26, 27, 40–44]. (It should be noted that alloy 1 also contained 0.22 wt% C, which was considerably higher than the 0.02 wt% C reported for the Fe–35Ni–10Cr–5Al-base alloy 881-1 in reference 36; which, further, used Zr and Y co-doping instead of the Hf and Y used in alloy 1. The Hf/C ratio in alloy 1 was <1 due to the high C content (Table 3) and may have further contributed to the poor oxidation resistance of this alloy by negating the beneficial effects of the Hf [38]).

Cross-section SEM images for the oxidized 35Ni-base alloys 3: (Fe–35Ni–25Cr–4Al), 4: (Fe–35Ni–25Cr–4Al + Nb,C), and 6: (Fe–35Ni–25Cr–4Al + Ti,C) are shown in Fig. 2. The baseline alloy 3 without Nb, Ti, or C additions formed a scale consistent with borderline alumina scale formation, as evidenced by substantial transient oxidation product rich in Al–Ni–Fe–Cr–O in the outer scale (susceptible to spallation) and inner alumina of borderline continuity and a complex morphology with many regions of internal intrusions evident (Fig. 2a). Elemental mapping by EDS (Fig. 3) revealed that in addition to the inward intrusions of alumina, there were occasional local regions with inward growing oxide rich in Al, Hf, Y, and Si, likely oxidized remnants of segregation/local second-phase intermetallic formation in the as-cast structure.

Increasing the Ni content of alloy 3 from 35 to 45 wt% in alloy 5 (Table 2) did not result in a transition to protective alumina scale formation, as evidenced by the

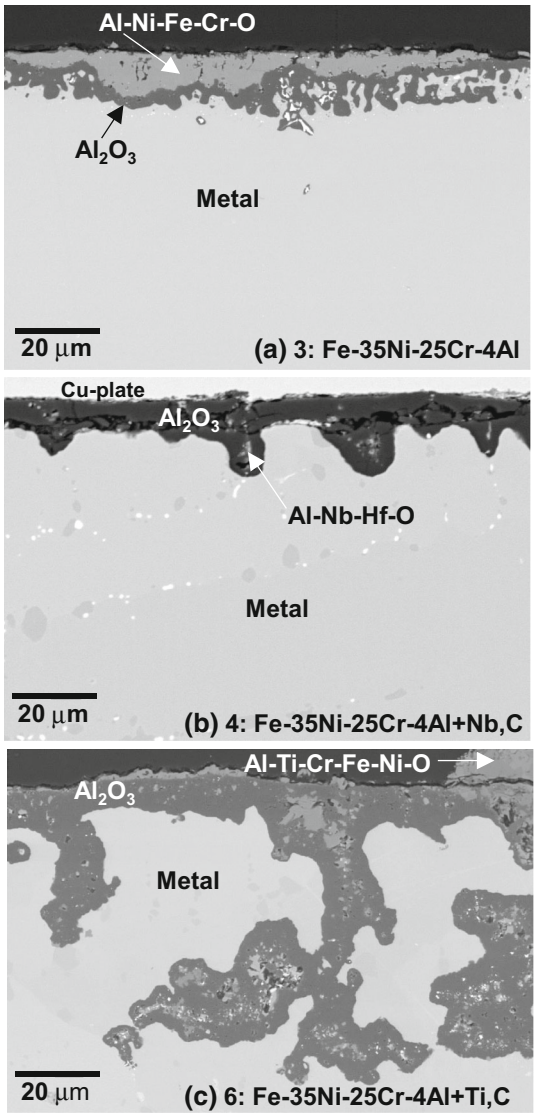

Fig. 2 SEM backscatter mode cross-sections of as-cast Fe–Ni–Cr–Al-based alloys after 1000 h (**a**, **c**) and 1200 h (**b**) at 1100 °C in air with 10% H_2O (100-h cycles)

mass loss observed at 1100 °C in air with 10% H_2O (Fig. 1). The addition of Ti and C to alloy 3, alloy 6 (Table 2), resulted in both transient Al–Ti–Cr–Fe–Ni–O oxidation products susceptible to spallation, and significant exacerbation of the inward protruding alumina morphology (Fig. 2c), extending ~50–75 microns into the alloy after 1000 h of exposure at 1100 °C in air with 10% H_2O. These intrusions were generally associated with Al and Ti oxides (Fig. 4).

In contrast, the addition of Nb and C to alloy 3, alloy 4 (Table 2), resulted in a continuous inner alumina scale (Figs. 1, 2b). Relatively minor inward growing alumina intrusions were also evident and were associated with casting segregation

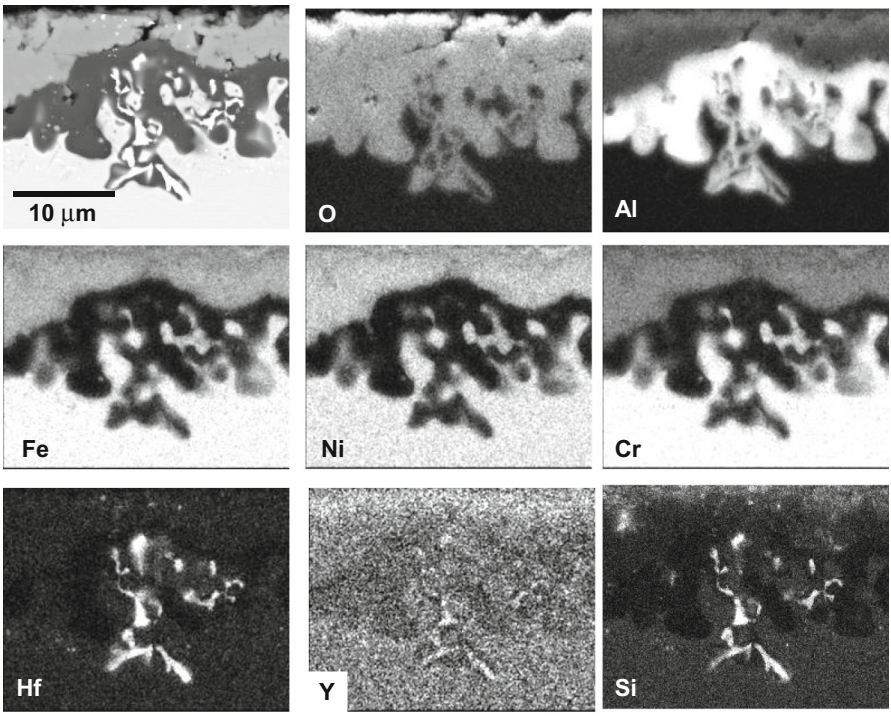

Fig. 3 SEM backscatter mode cross-section and elemental maps of oxide scale formed on as-cast Fe–Ni–Cr–Al-based alloy 3: Fe–35Ni–25Cr–4Al after 1000 h at 1100 °C in air with 10% H_2O (100-h cycles)

regions from local second-phase intermetallic precipitates. The alumina in these regions indicated prominent peaks in EDS spectra only for Al and O, although local fine areas also containing Al–Nb–Hf–O were also observed (Fig. 2b).

The low-positive mass gains and continuous alumina observed in cross-section indicate that alloy 4: Fe–35Ni–25Cr–4Al + Nb,C shows promise as an alloy base for future development to achieve a cast AFA alloy for use at 1100 °C. Further alloy optimization based on creep evaluation and longer-term oxidation exposures ($\gg$1000 h) will be needed. A potential concern with the high levels of 25 wt% Cr and 4 wt% Al employed in alloy 4 is that they are both strong BCC stabilizers that can also result in significant σ and related phase formation [7–9]. Although the intended application use temperature of 1100 °C is above that of the σ phase stability region, passing through this region during downtime cooling could potentially result in σ formation and decrease alloy ductility/toughness. Therefore, studies devoted to evaluation of lower levels of Cr in the alloy 4 base composition range are also of interest. Studies in relevant ethylene cracking and related environments to confirm both alumina scale formation and improved resistance to coking anticipated for AFA alloys are also needed.

From a fundamental perspective, the IOTT behavior of AFA alloys with increasing temperature and the beneficial effect of Nb + C and detrimental effect of Ti + C are not well understood. In the lower (20–25)Ni and (14–15)Cr AFA

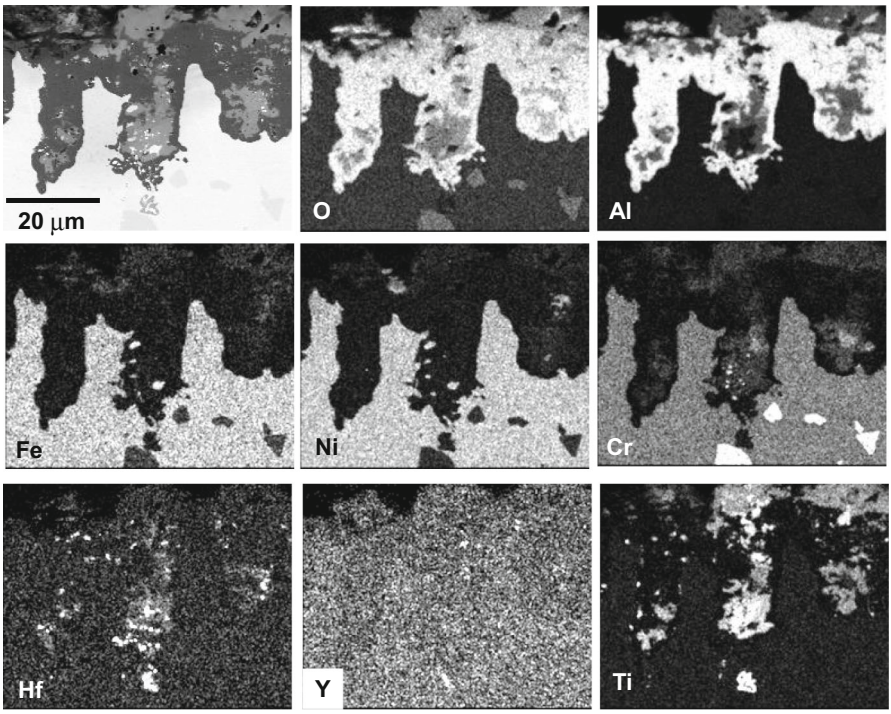

Fig. 4 SEM backscatter mode cross-section and elemental maps of oxide scale formed on as-cast Fe–Ni–Cr–Al-based alloy 6: Fe–35Ni–25Cr–4Al + Ti, C after 1000 h at 1100 °C in air with 10% H_2O (100-h cycles)

composition range at 650–800 °C in air with 10% H_2O, Nb additions were linked to increased Ni and Cr content in the austenite matrix phase [26], which contributed to increased IOTT (matrix phase composition can be critical to setting the transition between external and internal oxidation in multi-phase alloys, see References 45–47 for example). Prior work also speculated on second-phase precipitates, nanocarbides and/or intermetallics, potentially acting at local sites for H segregation during oxidation in water vapor, which may aide in amelioration of the detrimental effects of water vapor on IOTT [26, 27]. Quantitative assessment of the impact of Nb, Ti, and C additions on oxygen permeability and Al diffusivity in the austenite matrix phase based on Wagner internal/external oxidation theory [48] is a good starting place for gaining better understanding of their effects on IOTT. However, very recent studies [40, 41] have identified the volume fraction of oxide f_v variable from the classic Wagner treatment of the transition from internal to external oxidation [48] as playing a major role for internal/external oxidation of Ni-base alumina-forming alloys in steam. This framework may prove beneficial to improved understanding of the enhanced internal-like oxidation/morphological changes observed with inward protruding alumina when Ti versus Nb and C were added to the AFA alloys of the present work (Fig. 2).

Acknowledgements The authors thank C. Carmichael, M. Stephens, and T.M. Lowe for assistance with the experimental work. S. Dryepondt and M. Lance provided comments for the manuscript. This research was sponsored by Oak Ridge National Laboratory's Laboratory Directed Research and Development (LDRD) Technology Innovation Program and U.S. Department of Energy ARPA-E program. This manuscript has been authored by UT-Battelle, LLC under Contract No. DE-AC05-00OR22725 with the U.S. Department of Energy. The United States Government retains, and the publisher, by accepting the article for publication, acknowledges that the United States Government retains a non-exclusive, paid-up, irrevocable, world-wide license to publish or reproduce the published form of this manuscript, or allow others to do so, for United States Government purposes. The Department of Energy will provide public access to these results of federally sponsored research in accordance with the DOE Public Access Plan (http://energy.gov/downloads/doe-public-access-plan).

References

1. D. J. Young, *High Temperature Oxidation and Corrosion of Metals*, 2nd ed, (Elsevier, Oxford, 2016).
2. G. Y. Lai, *High-Temperature Corrosion and Materials Applications*, (ASM International, Materials Park, 2007).
3. H. Asteman, W. Hartnagel and D. Jakobi, *Oxidation of Metals* **80**, (1–2), 2013 (3–12). doi:10.1007/s11085-013-9381-3.
4. F. H. Stott, G. C. Wood and J. Stringer, *Oxidation of Metals* **44**, (1–2), 1995 (113–145). doi:10.1007/bf01046725.
5. S. Dryepondt, B. A. Pint and E. Lara-Curzio, *Materials Science and Engineering A: Structural Materials Properties Microstructure and Processing* **550**, 2012 (10–18). doi:10.1016/j.msea.2012.03.031.
6. A. Czyrska-Filemonowicz and B. Dubiel, *Journal of Materials Processing Technology* **64**, (1–3), 1997 (53–64). doi:10.1016/s0924-0136(96)02553-8.
7. Y. Yamamoto, M. P. Brady, Z. P. Lu, P. J. Maziasz, C. T. Liu, B. A. Pint, K. L. More, H. M. Meyer and E. A. Payzant, *Science* **316**, (5823), 2007 (433–436). doi:10.1126/science.1137711.
8. M. P. Brady, J. Magee, Y. Yamamoto, D. Helmick and L. Wang, *Materials Science and Engineering A: Structural Materials Properties Microstructure and Processing* **590**, 2014 (101–115). doi:10.1016/j.msea.2013.10.014.
9. Y. Yamamoto, M. P. Brady, M. Santella, H. Bei, P. Maziasz and B. Pint, *Metallurgical and Materials Transactions A: Physical Metallurgy and Materials Science* **42A**, (4), 2011 (922–931). doi:10.1007/s11661-010-0295-2.
10. X. Xu, X. Zhang, G. Chen and Z. P. Lu, *Materials Letters* **65**, (21–22), 2011 (3285–3288). doi:10.1016/j.matlet.2011.07.021.
11. J.-Y. Kang, H.-Y. Ha, M.-H. Jang, J. Moon, D.-W. Suh and T.-H. Lee, *Scripta Materialia* **102**, 2015 (63–66). doi:10.1016/j.scriptamat.2015.02.014.
12. S. H. Nie, Y. Chen, X. Ren, K. Sridharan and T. R. Allen, *Journal of Nuclear Materials* **399**, (2–3), 2010 (231–235).
13. L.-F. He, P. Roman, B. Leng, K. Sridharan, M. Anderson and T. R. Allen, *Corrosion Science* **82**, 2014 (67–76). doi:10.1016/j.corsci.2013.12.023.
14. D. Q. Zhou, W. X. Zhao, H. H. Mao, Y. X. Hu, X. Q. Xu, X. Y. Sun and Z. P. Lu, *Materials Science and Engineering A: Structural Materials Properties Microstructure and Processing* **622**, 2015 (91–100). doi:10.1016/j.msea.2014.11.013.
15. J. Ejenstam and P. Szakálos, *Journal of Nuclear Materials* **461**, 2015 (164–170).
16. B. Hu, G. Trotter, I. Baker, M. K. Miller, L. Yao, S. Chen and Z. Cai, *Metallurgical and Materials Transactions A* **46**, (8), 2015 (3773–3785).
17. G. Trotter and I. Baker, *Materials Science and Engineering A: Structural Materials Properties Microstructure and Processing* **627**, 2015 (270–276). doi:10.1016/j.msea.2014.12.072.
18. J. Zhang, P. Speck and D. J. Young, *Oxidation of Metals* **77**, (3–4), 2012 (167–187). doi:10.1007/s11085-011-9279-x.
19. D.-S. Li, Q.-X. Dai, X.-N. Cheng, R.-R. Wang and Y. Huang, *Journal of Iron and Steel Research International* **19**, (5), 2012 (74–78).
20. K. Zhao, H. Peng, X. Yang, G. Wang and Y. Wen, *Oxidtion of Metals* **83**, (3–4), 2015 (273–290). doi:10.1007/s11085-014-9520-5.

21. Y. F. Sun, Y. Z. Lv, Y. Zhang, J. Y. Zhao and Y. Wu, *Materials Science and Technology* **29**, (5), 2013 (511–516). doi:10.1179/1743284712y.0000000177.
22. X. Dong, L. Zhao, F. Sun, and L. Zhang, Strengthening of an Al-Containing Austenitic Stainless Steel at High Temperature, Paper No. GT2013-95494, pp. V05AT21A007. doi:10.1115/GT2013-95494
23. J. Hall, K. Hellström, J.-E. Svensson, M. Norell, M. Lundberg, T. Helander and L.-G. Johansson, *Oxidation of Metals* **82**, (3–4), 2014 (225–247). doi:10.1007/s11085-014-9489-0.
24. R. Elger and R. Pettersson, *Oxidation of Metals* **82**, (5–6), 2014 (469–490).
25. M. P. Brady, Y. Yamamoto, M. Santella and B. A. Pint, *Scripta Materialia* **57**, (12), 2007 (1117–1120). doi:10.1016/j.scriptamat.2007.08.032.
26. M. P. Brady, Y. Yamamoto, M. Santella and L. Walker, *Oxidation of Metals* **72**, (5–6), 2009 (311–333). doi:10.1007/s11085-009-9161-2.
27. M. P. Brady, K. Unocic, M. Lance, M. Santella, Y. Yamamoto and L. Walker, *Oxidation of Metals* **75**, (5–6), 2011 (337–357). doi:10.1007/s11085-011-9237-7.
28. P. Singh and N. Q. Minh, *International Journal of Applied Ceramic Technology* **1**, (1), 2004 (5–15). doi:10.1111/j.1744-7402.2004.tb00149.x.
29. R. Kirchheiner, D. J. Young, P. Becker, and R. N. Durham, Improved Oxidation and Coking Resistance of a New Alumina Forming Alloy 60 HT for the Petrochemical Industry, CORROSION 2005 Paper No. 05428 (NACE 2005, Houston).
30. H. Asteman, P. Keil, W. Hartnagel, E. Müller-Lorenz, and D. Jakobi, High Temperature Corrosion of Burner Tube Alloys Exposed to Flue Gas and Reducing Atmosphere Used for Annealing-A Laboratory Study CORROSION 2011 Paper 11191 (NACE 2011, Houston).
31. D. Jakobi, P. Karduck, and A. Freiherr von Richthofen, The High-Temperature Corrosion Resistance of Spun-Cast Materials for Steam-Cracker Furnaces: A Comparative Study of Alumina- and Chromia-Forming Alloys" CORROSION 2013 Paper No. 2287 (NACE 2013, Houston).
32. CENTRALLOY® HT E (Cast Austenitic Stainless Steel), Alloy Digest, Copyright© 2013, ASM International
33. G. Muralidharan, Y. Yamamoto, M. P. Brady, B. A. Pint, D. Voke, and R. I. Pankiw, Development of Cast Alumina-forming Austenitic Stainless Steel Alloys for use in High Temperature Process Environments, CORROSION 2015, Paper No. 6114 (NACE 2015, Houston).
34. J. C. Pivin, D. Delaunay, C. Roquescarmes, A. M. Huntz and P. Lacombe, *Corrosion Science* **20**, (3), 1980 (351–373). doi:10.1016/0010-938x(80)90005-0.
35. N. Belen, P. Tomaszewicz and D. J. Young, *Oxidation of Metals* **22**, (5–6), 1984 (227–245). doi:10.1007/bf00656577.
36. V. Ramakrishnan, J. A. McGurty and N. Jayaraman, *Oxidation of Metals* **30**, (3–4), 1988 (185–200). doi:10.1007/bf00666596.
37. G. Muralidharan, Y. Yamamoto, and M. P. Brady, US Patent 8,431,072 "Cast Alumina Forming Austenitic Stainless Steels" (April 30, 2013).
38. B. A. Pint, *Journal of ACERS* **86**, 2003 (686–695).
39. G. Muralidharan, Y. Yamamoto, M. P. Brady, L. R. Walker, H. M. Meyer III and D. N. Leonard, *JOM* **68**, (11), 2016 (2803–2810). doi:10.1007/s11837-016-2094-8.
40. W. Zhao and B. Gleeson, *Oxidation of Metals* **79**, (5–6), 2013 (613–625). doi:10.1007/s11085-013-9359-1.
41. W. Zhao and B. Gleeson, *Oxidation of Metals* **83**, (5–6), 2015 (607–627). doi:10.1007/s11085-015-9541-8.
42. E. Essuman, G. H. Meier, J. Zurek, M. Hansel and W. J. Quadakkers, *Oxidation of Metals* **69**, (3–4), 2008 (143–162). doi:10.1007/s11085-007-9090-x.
43. R. Janakiraman, G. H. Meier and F. S. Pettit, *Metallurgical and Materials Transactions A* **30**, (11), 1999 (2905–2913).
44. J. L. Smialek, *JOM* **58**, (1), 2006 (29–35).
45. F. Gesmundo, F. Viani and Y. Niu, *Oxidation of Metals* **42**, (5–6), 1994 (409–429).
46. F. Gesmundo and B. Gleeson, *Oxidation of Metals* **44**, (1–2), 1995 (211–237). doi:10.1007/bf01046728.
47. R. N. Durham, B. Gleeson and D. J. Young, *Oxidation of Metals* **50**, (1–2), 1998 (139–165). doi:10.1023/a:1018880019395.
48. C. Wagner, *Zeitschrift Fur Elektrochemie* **63**, (7), 1959 (772–790).